Semiconductor Physics, Quantum Electronics & Optoelectronics, 2021. V. 24, No 1. P. 16-21.

Semiconductor physics

Modified expressions of field and thermionic-field emission for Schottky barrier diodes in the reverse regime

A. Latreche

LPMRN Laboratory, Department of Materials Science, Faculty of Sciences and Technology,
University of Mohamed El Bachir El Ibrahimi,
Bordj-Bou-Arreridj 34030, Algeria
E-mail: hlat26@ yahoo.fr.

Abstract. In this theoretical work, the author has modified the current-voltage relationship of the field and thermionic–field emission models developed by Padovani and Stratton for the Schottky barrier diodes in the reverse bias conditions with account of the image force correction. Considered in this approach has been the shape of Schottky barrier as trapezoidal. The obtained results show a good agreement between current densities calculated within the framework of these developed models and those calculated using the general model.

Keywords: tunneling current, field emission, thermionic–field emission, Schottky diode, image force barrier lowering, trapezoidal barrier.

https://doi.org/10.15407/spqeo24.01.016
PACS 85.30.De, 85.30.Kk, 85.30.Mn

Manuscript received 23.11.20; revised version received 28.12.20; accepted for publication 10.02.21; published online 09.03.21.

1. Introduction

In recent years, silicon carbide (4H-SiC), gallium oxide (Ga_2O_3) and other wide bandgap semiconductors became promising for next-generation power electronic devices because of their excellent material properties for high-voltage applications [1–4]. Under the reverse bias condition, the dominant mechanisms, by which the carrier transport occurs in Schottky barriers, are thermionic emission at low bias and carrier tunneling through the potential barrier at high bias voltages [5–16]. The image force lowering of the potential energy barrier is important for wide bandgap semiconductor Schottky barrier diodes due to the high electric fields at the metal-semiconductor interface [16]. The most significant generally term that causes the effective barrier height to differ from the flat-band barrier height is the image force lowering of the potential energy barrier [16]. An accurate analytical model to describe the reverse characteristics of Schottky barrier diodes, which takes into account the image force correction, is necessary. The most sufficient analytical model for describing the reverse tunneling current is the Padovani–Stratton model [17], however, this model does not include the image force correction, although some authors [9, 14, 18, 19] used it without demonstration, on the condition that they replaced the barrier height ϕ_b by the barrier height reduced by image force effect, $\phi_b - \Delta\phi_b$. In our recent work [20], we demonstrated that this method is inaccurate. In this work, we will develop an analytical model to describe the reverse tunneling current by taking into account the Schottky barrier lowering caused by the image force effect. With this aim, we assume that the shape of the Schottky barrier is trapezoidal.

2.Theory and modeling

The current density due to the net flow of electrons from the metal to semiconductor through the Schottky barrier is given in [21, 22]

$$J_{Tun} = \frac{A^* T^2}{k_B} \int_0^{U_{max}} T(E_x) \ln\left(\frac{1+\exp\left(-q\varsigma - E_x\right)/k_B T}{1+\exp\left(-q\varsigma - qV_R - E_x\right)/k_B T} \right) dE_x. \quad (1)$$

Here, k_B, T, and A^* are the Boltzmann constant, temperature, and effective Richardson constant, respectively. ζ denotes the difference between the equilibrium Fermi level and conduction bands, and $T(E_x)$ is the tunneling probability that electron at the energy level E_x can penetrate the potential barrier. In this study the probability is derived on the basis of the WKB approximation and given by

$$T_{WKB}(E_x) = \exp\left[-2 \int_{x_1}^{x_2} \left(\frac{2m^*}{\hbar^2} \left(U(x) - E_x \right) \right)^{1/2} dx \right], \quad (2)$$

where x_1 and x_2 are the classical boundaries at any given

electron energy E_x. The WKB approximation enables to calculate the tunneling current through a Schottky barrier with reasonable accuracy [23]. $U(x)$ is the potential energy profile for the Schottky barrier diode. With account of barrier lowering caused by the image force, the potential energy of the Schottky barrier $U(x)$ measured with respect to the energy of the bottom of conduction band in the bulk of semiconductor can be expressed as [24]

$$U(x)=\frac{q^2N_D}{2\varepsilon_S}(D-x)^2-\frac{q^2}{16\pi\varepsilon_S x}, \tag{3}$$

where N_D, ε_S are the doping concentration and the semiconductor permittivity, respectively. The depletion width D depends on the electric field F (bias voltage, V) as

$$D=\sqrt{\frac{2\varepsilon_S(\phi_b-\varsigma-V)}{qN_D}}=\frac{\varepsilon_S F}{qN_D}. \tag{4}$$

Taking into account the image force correction, we will assume that the shape of the Schottky barrier is trapezoidal as shown in Fig. 1. Neglecting the image force correction, the Schottky barrier can be approximated as a triangular barrier, as shown in the same figure.

The trapezoidal Schottky barrier shown in Fig. 1 has the following form:

$$U(x)=\begin{cases} E_f+\dfrac{q\phi_b-q\Delta\phi_b}{x_m}x, & 0\le x\le x_m \\ E_f+q\phi_b-q\Delta\phi_b, & x_m\le x\le x_0 \\ E_f+q\phi_b-qFx, & x_0\le x \end{cases} \tag{5}$$

where $x_m=q\Delta\phi_b/2qF$ and $x_0=q\Delta\phi_b/qF$ are the abscissas of the potential maximum in the presence of image barrier lowering and the potential, when the image force is negligible at the electron energy $E_x=E_f+q\phi_b-q\Delta\phi_b$, respectively, and they depend on the electric field F. The barrier drop ($\Delta\phi_b$) due to the image charge effect is given by [25]

$$\Delta\phi_b=\left[\frac{q^3N_D(\phi_b-\varsigma-V)}{8\pi^2\varepsilon_S^3}\right]^{1/4}. \tag{6}$$

The tunneling probability $T(E_x)$, under the WKB approximation through the trapezoidal potential can be evaluated by multiplication of the three probabilities in each region of the trapezoidal potential and can be expressed as

$$\ln[T(E_x)]=\ln[T_1(E_x)\times T_2(E_x)\times T_3(E_x)]= \\ =-\alpha_1\left(\frac{2\alpha_2}{3}A^{3/2}+\frac{1}{2}q\Delta\phi_b A^{1/2}\right), \tag{7}$$

where A, α_1, and α_2 are given by

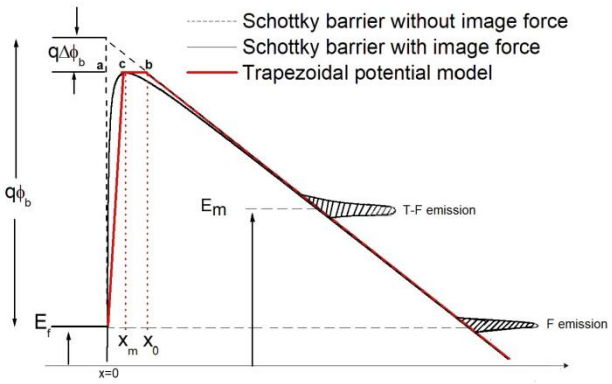

Fig. 1. Schematic energy level diagrams showing thermionic–field emission, and field emission for a Schottky barrier under the reverse bias voltage.

$$A=E_f-E_x+q\phi_b-q\Delta\phi_b, \tag{8}$$

$$\alpha_1=\frac{2\sqrt{2m^*}}{\hbar qF}, \tag{9}$$

$$\alpha_2=1+\frac{q\Delta\phi_b}{2(q\phi_b-q\Delta\phi_b)}. \tag{10}$$

In the notation of Padovani and Stratton [17], and neglecting the parameter ζ before the applied voltage (V), the parameter α_1 can be written by another way as

$$\alpha_1=\frac{1}{E_{00}(q\phi_b-qV)^{1/2}}, \tag{11}$$

in which the energy E_{00} is given by [17]:

$$E_{00}=\frac{h}{4\pi}\left(\frac{N_D}{m^*\varepsilon_S}\right). \tag{12}$$

Field emission: Low-temperature range

Field emission (FE) occurs when electrons tunnel at the Fermi level of the metal, it dominates when the applied field is high enough or at low temperatures. Stratton [17, 26] derived the current-voltage relationship for field emission through a potential barrier of arbitrary shape, and it can be expressed for sufficiently large biases ($c_1V >> 1$) as

$$J_{FE}=\frac{A^*\pi T}{c_1k_B}\frac{e^{-b_1}}{\sin(\pi c_1k_BT)}, \tag{13}$$

where the parameters b_1 and c_1 are the first two terms of the Taylor expansion for the exponent of the tunneling probability $T(E_x)$ for the barrier around the Fermi level. By letting $\varepsilon_x = E_f - E_x$, the equation (7) may be expanded in the Taylor series as

$$\ln[T(E_x)]=-\left[b_1+c_1\varepsilon_x+f_1\varepsilon_x^2+...\right]. \tag{14}$$

Here,

$$b_1 = \alpha_1 (q\phi_b - q\Delta\phi_b)^{1/2} \left[\frac{2}{3} q\phi_b + \frac{1}{6} q\Delta\phi_b \right], \quad (15)$$

$$c_1 = \alpha_1 (q\phi_b - q\Delta\phi_b)^{1/2} \left[\frac{3}{2}\alpha_2 - \frac{1}{2} \right], \quad (16)$$

$$f_1 = \frac{4q\phi_b - 3q\Delta\phi_b}{16(q\phi_b - q\Delta\phi_b)^{3/2}} \alpha_1 . \quad (17)$$

The equation (13) of the field emission will be valid only for temperatures like that [17]

$$k_B T < \frac{1}{c_1 + (2 f_1)^{1/2}}. \quad (18)$$

Neglecting the image force correction ($\Delta\phi_b = 0$) in the equations (15) and (16), we find the same expression of the Padovani–Stratton for the field emission mode [17]:

$$J_{FE} = \frac{A^* T^2 \pi E_{00} \exp\left[-2q\phi_b^{3/2} / 3E_{00} (\phi_b - V)^{1/2} \right]}{k_B T \left[\phi_b / (\phi_b - V) \right]^{1/2} \sin\left\{ \pi k_B T \left[\phi_b / (\phi_b - V) \right]^{1/2} / E_{00} \right\}}. \quad (19)$$

Thermionic–field emission: Intermediate temperature range

If the temperature is raised, electrons are excited to higher energies, and the tunneling probability increases rapidly because these electrons "see" a thinner and lower barrier [5]. So, most of emitted electrons tunnels at the energy E_m between the top of the Schottky barrier and Fermi level energy. The energy distribution of emitted electrons can be approximated as a Gaussian distribution, and the energy level E_m is its mean, where the contribution to the tunneling current is maximum. By putting $\varepsilon = E_m - E_x$ and following the same steps for FE model, the exponent of the transparency for the barrier around the particular energy E_m, and neglecting the error function term, the current density of thermionic–field emission (TFE) could be expressed as [17, 27]

$$J_{TFE} = \frac{A^* T}{2k_B} \left(\frac{\pi}{|f_m|} \right)^{1/2} e^{\left(\frac{E_f - E_m}{k_B T} - b_m \right)}, \quad (20)$$

where the parameters b_m, c_m, and f_m are the first three terms of the Taylor expansion for the exponent of the tunneling probability $T(E_x)$ for the barrier around the energy E_m, and they can be expressed as

$$b_m = \alpha_1 \left[\frac{2\alpha_2}{3} B^{3/2} + \frac{q\Delta\phi_b}{2} B^{1/2} \right], \quad (21)$$

$$c_m = \alpha_1 \left[\alpha_2 B^{1/2} + \frac{q\Delta\phi_b}{4B^{1/2}} \right], \quad (22)$$

$$f_m = \alpha_1 \left[\frac{\alpha_2}{4B^{1/2}} - \frac{q\Delta\phi_b}{16B^{3/2}} \right]. \quad (23)$$

Here, the parameter B is given by

$$B = E_f - E_m + q\phi_b - q\Delta\phi_b . \quad (24)$$

The energy level E_m that represents the peak of the energy distribution for emitted electrons will be as follows [17]

$$c_m k_B T = 1. \quad (25)$$

Using the equations (22) and (25), and after some manipulations, we can find an equation of the second-order for the parameter B, the solution of this equation can be given by

$$B = \frac{1 - \frac{1}{2}\alpha_2 q\Delta\phi_b (\alpha_1 k_B T)^2 + \sqrt{1 - \alpha_2 q\Delta\phi_b (\alpha_1 k_B T)^2}}{2\alpha_2^2 (\alpha_1 k_B T)^2}. \quad (26)$$

From the equation (24), the energy E_m is expressed as

$$E_m = E_f + q\phi_b - q\Delta\phi_b - B. \quad (27)$$

The equation of the second order for the parameter B has a real solution, if the condition given by Eq. (28) is satisfied; this means that the energy level E_m is located below the top of barrier:

$$1 \geq \alpha_2 q\Delta\phi_b (\alpha_1 k_B T)^2. \quad (28)$$

The minimum bias to be applied for observing the thermionic–field emission current is as follows:

$$-V \approx \left(\frac{q^3 N_D}{8\pi^2 \varepsilon_S^3} \right)^{1/3} \left(\frac{k_B T}{E_{00}} \right)^{8/3}. \quad (29)$$

Neglecting the image force correction ($\Delta\phi_b = 0$) in the equations (21) and (23), we find another expression for thermionic–field emission, which can be written as

$$J_{TFE} = J_S e^{-e_0 \frac{qV}{k_B T}}, \quad (30)$$

$$J_S = \frac{A^* T}{k_B} E_{00} \left[\frac{\pi}{k_B T} (q\phi_b - qV) \right]^{1/2} e^{-e' \frac{q\phi_b}{k_B T}}, \quad (31)$$

$$e_0 = \frac{1}{3} \left(\frac{E_{00}}{k_B T} \right)^2, \quad (32)$$

$$e' = 1 - e_0. \quad (33)$$

3. Results and discussion

To examine the accuracy of our new model, we compare it with its original one that has been deduced from the equation (1). We will perform our simulation of reverse characteristics by using the SiC Schottky diode, where the effective mass $m^* = 0.2m_0$, and effective Richardson constant is equal to 146 $A \cdot cm^{-2} \cdot K^{-2}$ [28, 29]. The barrier height is equal to $\phi_b = 1.1$ V, and our calculations are performed over large bias voltages, up to −1000 V at room temperature. For thermionic–field emission current, we used the doping concentration close to $N_d = 5 \cdot 10^{15}$ cm^{-3}, while, for the field emission current, we used the doping concentration $N_d = 2 \cdot 10^{17}$ cm^{-3}. Fig. 2 shows for comparison the current densities calculated using our developed model for field emission and thermionic–field emission as well as current densities calculated using the general model given by the equation (1). It is clear from this figure that the current densities of FE and TFE are in good agreement with those calculated using the general model (Eq. (1)), in particular FE current over all the range of reverse bias voltages. For low and high bias voltages, the calculations exhibit a discrepancy between our TFE model and the general model. For low bias voltages, the energy E_m is located at the top of barrier, so, the Taylor expansion for the exponent of the tunneling probability $T(E_x)$ of the barrier around the energy E_m is not accurate, because the value of the quantity B has the same order of magnitude of the energy $\varepsilon = E_m - E_x$, hence, the Taylor expansion with the first three terms in this case is not satisfied [21]. For high bias voltages, the energy E_m is getting closer to the Fermi energy where the field emission becomes the dominant process.

The shape of the trapezoidal barrier shown in Fig. 1 is not the only possible trapezoidal shape that can describe the Schottky barrier with image force correction. In fact, we can modify the trapezoidal barrier sketched in Fig. 1 by varying the intermediate point c between the two extreme points a and b, which have the abscissas $x = 0$ and $x = x_0$, respectively. The abscissa of the new point c can be determined by a fractional number multiplied by the abscissa x_m as $0x_m$, $(1/3)x_m$, $(1/2)x_m$, $(2/3)\,x_m$, $(3/4)x_m$, $1x_m$ and $(5/4)x_m$. The trapezoidal barrier defined by $x_c = 0x_m$ was already used to describe the reverse current characteristics for 4H-SiC Schottky diodes [30].

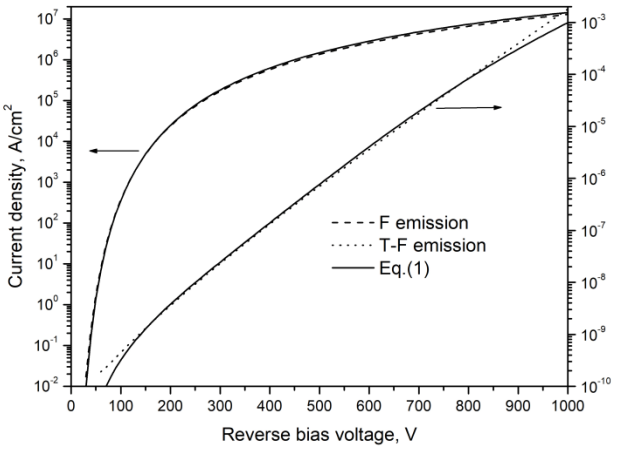

Fig. **2.** Calculated reverse current densities according to general model (Eq. (1)), TFE/FE models for 4H-SiC SBD with account of the image force correction.

In Fig. 3, we have shown the percent error in the current density $\left(J_{TFE/FE} - J_{Eq.(1)}\right) / J_{Eq.(1)}$ for each new point c for field and thermionic–field emission. As shown in Fig. 3a, the trapezoidal barrier defined by the point c that has the abscissa $(5/4)x_m$ is better than other abscissas in the case of field emission, and the mean percent error is close to 8%. The mean percent error in the current density of the trapezoidal barrier defined by the point c that has the abscissa $1x_m$ is close to 9%, which means that it is in good agreement with the trapezoidal barrier defined by the abscissa $(5/4)x_m$.

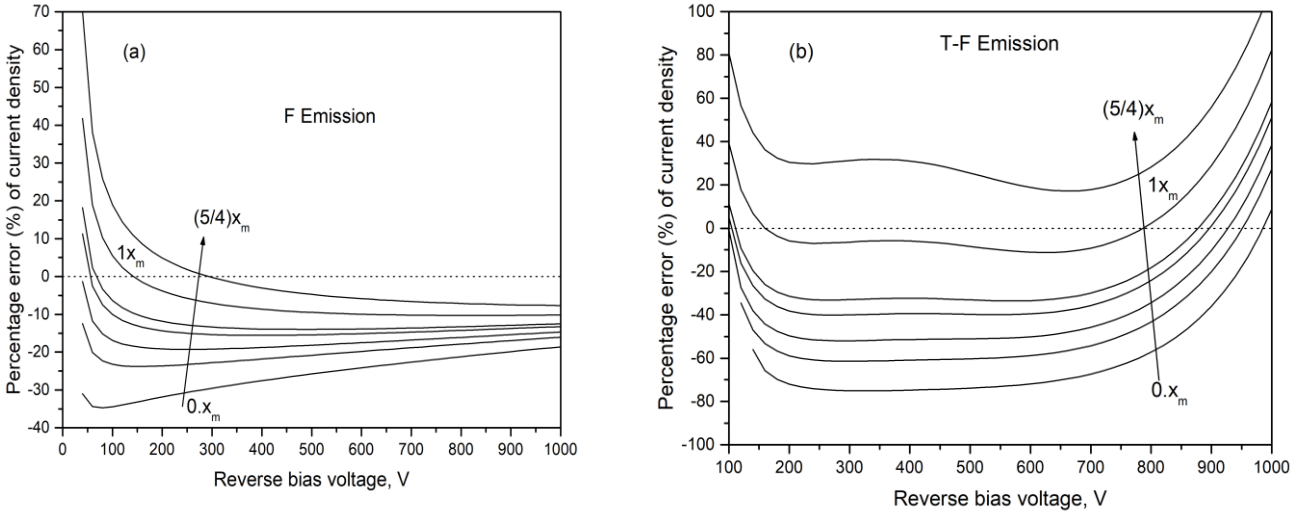

Fig. 3. Percentage error (%) of current density with the image force barrier lowering according to FE (a) and TFE (b) models for 4H-SiC SBD at various abscissas of the point c.

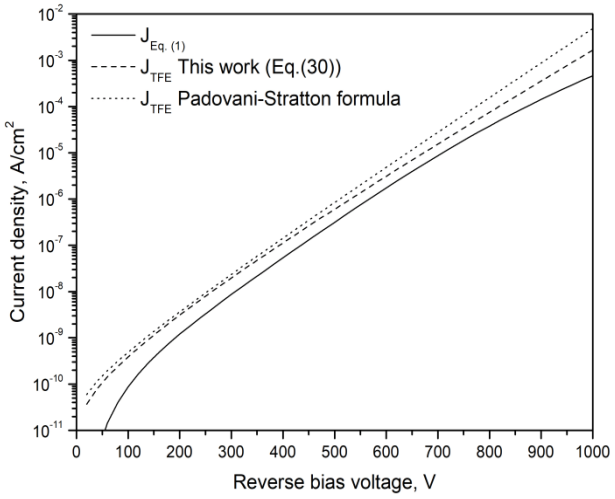

Fig. 4. Dependences of current density on the reverse bias voltage for the Padovani–Stratton TFE and our TFE models without image force correction.

The expressions of parameters b_1, c_1, and f_1 when the trapezoidal barrier is defined by the abscissa $(5/4)x_m$ are changed and can be given by the expressions:

$$b_1 = \alpha_1 \left(q\phi_b - q\Delta\phi_b\right)^{1/2} \left[\frac{2}{3} q\phi_b + \frac{1}{8} q\Delta\phi_b\right], \tag{34}$$

$$c_1 = \alpha_1 \left(q\phi_b - q\Delta\phi_b\right)^{1/2} \left[\frac{13}{8}\alpha_2 - \frac{5}{8}\right], \tag{35}$$

$$f_1 = \frac{\left(16q\phi_b - 9q\Delta\phi_b\right)}{16\left(q\phi_b - q\Delta\phi_b\right)^{3/2}} \alpha_1 . \tag{36}$$

In the case of thermionic–field emission (Fig. 3b), the trapezoidal barrier defined by the abscissa $1x_m$ is better than the other ones.

In Fig. 4, we show for comparison the current density calculated using our new model (Eq. (30)) for thermionic–field emission and that calculated by Padovani–Stratton (Eq. (49) in Ref. [17]), when the image force is neglected. As shown in this figure, the current density of our new TFE model is closer to the general model (1) than the Padovani–Stratton one, in particular, for high reverse bias voltages.

4. Conclusion

In this study, we have modeled the Schottky barrier by a trapezoidal barrier for developing a new analytical model to describe the tunneling reverse characteristics, when the image force correction is taken into account. The voltage-current relationships have been derived for field and thermionic–field emission in the reverse regime. Our results are in good agreement with those obtained by the general model.

References

1. Kimoto T. Material science and device physics in SiC technology for high-voltage power devices. *Jpn. J. Appl. Phys.* 2015. **54**. P. 040103. https://doi.org/10.7567/JJAP.54.040103.
2. Privitera S.M.S., Latrice G., Camarda M., Piluso N., and La Via F. Electrical properties of extended defects in 4H-SiC investigated by photoinduced current measurements. *Appl. Phys. Exp*. 2017. **10**. P. 036601. https://doi.org/10.7567/APEX.10.036601.
3. Stepanov S.I., Nikolaev V.I., Bougrov V.E. and Romanov A.E. Gallium oxide: properties and applications – a review. *Rev. Adv. Matter Sci*. 2016. **44**. P. 63–86.
4. Pearton S.J., Jiancheng Yang J., Cary P.H. *et al.* A review of Ga_2O_3 materials, processing, and devices. *Appl. Phys. Rev*. 2018. **5**. P. 011301. https://doi.org/10.1063/1.5006941.
5. Rhoderick E.H. Metal-semiconductor contacts. *IEEPROC.* 1982. **129**. P. 1–14.
6. Latreche A. Combined thermionic emission and tunneling mechanisms for the analysis of the leakage current for Ga_2O_3 Schottky barrier diodes. *SN Appl. Sci*. 2019. **1**. P. 188. https://doi.org/10.1007/s42452-019-0192-2.
7. Latreche A. Conduction mechanisms of the reverse leakage current of β-Ga_2O_3 Schottky barrier diodes. *SPQEO*. 2019. **22**. P. 19−25. https://doi.org/10.15407/spqeo22.04.397.
8. Latreche A. Conduction mechanisms of the reverse leakage current of 4H-SiC Schottky barrier diodes. *Semicond. Sci. Technol*. 2019. **34**. P. 025016. https://doi.org/10.1088/1361-6641/aaf8cb.
9. Hatakenama T. and Shinohe T. Reverse characteristics of a 4H-SiC Schottky barrier diode. *Mater. Sci. Forum*. 2002. **389–393**. P. 1169–1172. https://doi. org/ 10.4028/www.scientific.net/MSF.389-393.1169.
10. Latreche A. Combination of thermionic emission and tunneling mechanisms to analyze the leakage current in 4H-SiC Schottky barrier diodes. *SPQEO*. 2019. **22**. P. 19−25. https://doi.org/10.15407/spqeo22.01.20.
11. Blasciuc-Dimitriu D., Horsfall A.B., Wright N.G. *et al.* Quantum modeling of *I–V* characteristics for 4H–SiC Schottky barrier diodes. *Semicond. Sci. Technol.* 2005. **20**. P. 10–15. https://doi.org/10.1088/0268-1242/20/1/002.
12. Furno M., Bonani F. and Ghione G. Transfer matrix method modelling of inhomogeneous Schottky barrier diodes on silicon carbide. *Solid-State Electron.* 2007. **51**. P. 466−474. https://doi.org/10.1016/j.sse.2007.01.028.
13. Treu M., Rupp R., Kpels H. and Bartsch W. Temperature dependence of forward and reverse characteristics of Ti, W, Ta and Ni Schottky diodes on 4H-SiC. *Mater. Sci. Forum.* 2001. **353-356**. P. 679–682. https://doi.org/10.4028/ www.scientific.net/MSF.353-356.679.

14. Higashiwaki M., Konishi K., Sasaki K. *et al*. Temperature-dependent capacitance–voltage and current–voltage characteristics of Pt/Ga_2O_3 (001) Schottky barrier diodes fabricated on *n*–Ga_2O_3 drift layers grown by halide vapor phase epitaxy. *Appl. Phys. Lett*. 2016. **108**. P. 133503. https://doi.org/10.1063/1.4945267.
15. Okino H., Kameshiro N., Konishi K. *et al*. Analysis of high reverse currents of 4H-SiC Schottky-barrier diodes. *J. Appl. Phys.* 2017. **122**. P. 235704. https://doi.org/10.1063/1.5009344.
16. Crofton J. and Sriram S. Reverse leakage current calculations for SiC Schottky contacts. *IEEE Trans. Electron. Devices*. 1996. **43**. P. 2305–2307. https://ieeexplore.ieee.org/document/544427.
17. Padovani F.A. and Stratton R. Field and thermionic field emission in Schottky barriers. *Solid-State Electron.* 1962. **9**. P. 695–707. https://doi.org/10.1016/0038-1101(66)90097-9.
18. Umezawa H., Saito T., Tokuda N. *et al.* Leakage current analysis of diamond Schottky barrier diode. *Appl. Phys. Lett.* 2007. **90**. P. 073506. https://doi.org/10.1063/1.2643374.
19. Kiziroglou M.E., Li X., Zhukov A.A. *et al.* Thermionic field emission at electrodeposited Ni–Si Schottky barriers. *Solid-State Electron.* 2008. **52**. P. 1032–1038. https://doi.org/10.1016/j.sse.2008.03.002.
20. Latreche A. Validity of the Padovani–Stratton formulas for analysis of reverse current–voltage characteristics of 4H–SiC Schottky barrier diodes. *Semicond. Sci. Technol*. 2019. **34**. P. 055021. https://doi.org/10.1088/1361-6641/ab1191.
21. Tsu R. and Esaki L. Tunneling in a finite superlattice. *Appl. Phys. Lett.* 1973. **22**. P. 562–564. https://doi.org/10.1063/1.1654509.
22. Eriksson J., Rorsman N. and Zirath H. 4H-silicon carbide Schottky barrier diodes for microwave applications. *IEEE Trans. Microwave Theory Technol*. 2003. **51**. P. 796–804. https://doi.org/10.1109/TMTT.2003.808610.
23. Latreche A. and Ouennoughi Z. Modified Airy function method modelling of tunnelling current for Schottky barrier diodes on silicon carbide. *Semicond. Sci. Technol*. 2013. **28**. P. 105003. https://doi.org/10.1088/0268-1242/28/10/105003.
24. Zheng L., Joshi R.P. and Fazi C. Effects of barrier height fluctuations and electron tunnelling on the reverse characteristics of 6H–SiC Schottky contacts. *J. Appl. Phys.* 1999. **85**. P. 3701–3707. https://doi.org/10.1063/1.369735.
25. Rhoderick E.H. and Williams R.H. *Metal–Semiconductor Contact.* Oxford: Oxford University Press, 1988.
26. Stratton R. Volt-current characteristics for tunneling through insulating films. *J. Phys. Chem. Solids*. 1962. **23**. P. 1177–1190. https://doi.org/10.1016/0022-3697(62)90165-8.
27. Stratton R. Theory of field emission from semiconductors. *Phys. Rev*. 1962. **125**. P. 67–82. https://doi.org/10.1103/PhysRev.125.67.
28. Itoh A. and Matsunami H. Analysis of Schottky barrier heights of metal/SiC contacts and its possible application to high-voltage rectifying devices. *phys. status solidi (a)*. 1997. **162**. P. 389–408. https://doi.org/10.1002/1521-396X(199707)162:1<389::AID-PSSA389>3.0.CO;2-X.
29. Roccaforte F. Richardson's constant in inhomogeneous silicon carbide Schottky contacts. *J. Appl. Phys.* 2003. **93**. P. 9137–9144. https://doi.org/10.1063/1.1573750.
30. Nicholls J. R., Dimitrijev S. A compact model for SiC Schottky barrier diodes based on the fundamental current mechanisms. *IEEE Journal of the Electron Devices Society*. 2020. **8**. P. 545. https://ieeexplore.ieee.org/document/9081977.

Author and CV

Abdelhakim Latreche is a professor of the Department of Materials Science at the University of Mohamed El Bachir El Ibrahimi, Algeria. His main research interests include the electrical characterization and simulation of semiconductor devices, in particular, wide gap (SiC, Ga_2O_3, ...) Schottky barrier diodes.

Модифіковані рівняння польового та термоіонно-польового випромінювання для бар'єрних діодів Шотткі у зворотному режимі

A. Latreche

Анотація. У цій теоретичній роботі автор модифікував співвідношення струм-напруга у моделях польового та термоіонно-польового випромінювання, розроблених Падовані та Страттоном для бар'єрних діодів Шотткі в умовах зворотного зміщення з урахуванням корекції сил зображення. У цьому підході розглянуто форму бар'єра Шотткі як трапецієподібну. Отримані результати добре узгоджуються з густинами струму, розрахованими в рамках цих розроблених моделей, та тими, що розраховуються за загальною моделлю.

Ключові слова: тунельний струм, польове випромінювання, термоіонно-польове випромінювання, діод Шотткі, сили зображення, трапецієподібний бар'єр.